Field Experiments of LTE-Advanced-Based 8×8 Multiuser MIMO System with Vector Perturbation

Satoshi Sonobe, Satoshi Tsukamoto, Takahiro Maeda, Kazuto Yano, Hiroshi Ban, Masahiro Uno, Kiyoshi Kobayashi
ATR Wave Engineering Laboratories, Kyoto, Japan
{sonobe, tsukamoto, maeda, kzyano, hban, uno, kobayashi}@atr.jp

***Abstract*— We have developed an LTE-Advanced-based 8×8 multiuser MIMO experimental system with vector perturbation to overcome performance degradation of the MIMO technique under spatially correlated channel conditions, such as a line-of-sight (LoS) environment. This paper introduces our experimental system and shows results of outdoor/indoor experiments envisioning small-cell environments. Through experimental evaluation, it is confirmed that the throughput of the downlink transmission with vector perturbation reaches almost double that with MMSE spatial filtering.**

I. Introduction

The mobile communications system is now experiencing an explosive increase in traffic as the number of users augments and the use of smartphones spreads. This trend will be predicted to accelerate in the years to come. Achieving a significant improvement of traffic capacity in the mobile communications system is therefore an urgent matter.

A variety of techniques have been studied for improving the area spectral efficiency of the mobile communications system. Among these, two key techniques are expected to be effective in this regard. One is reducing cell size with the aim of decreasing the number of active users per base station (BS) and reducing propagation loss between the BS and user equipment (UE). The other is enhancing multiuser multiple-input multiple-output (MU-MIMO) transmission [1] to simultaneously improve both total throughput within a cell and throughput of each UE.

In the case of MU-MIMO transmission in the downlink in a typical cellular system in which the number of antenna elements of each UE is less than that of the BS, stream separation can be achieved by precoding the transmission signal on the BS side. Among several precoding schemes, minimum mean square error (MMSE) spatial filtering, a type of linear precoding, is one of the simple techniques [1], [2].

Although the spatial filtering can obtain high beamforming gain when channel correlation between receiver antennas is small, beamforming gain will be small in the case of high channel correlation. To compensate this drop in gain, the norm of antenna weight vectors of streams having small beamforming gain must be made large. However, as the total transmission power of a transmitter has an upper limit, this measure degrades power efficiency in the transmitter resulting in a drop in sum rate [3]. If the number of active users in a cell is large, this problem can be avoided by selecting and pairing users having small channel correlation. In a small cell environment having a small number of active users, however, such combinations of users cannot necessarily be obtained.

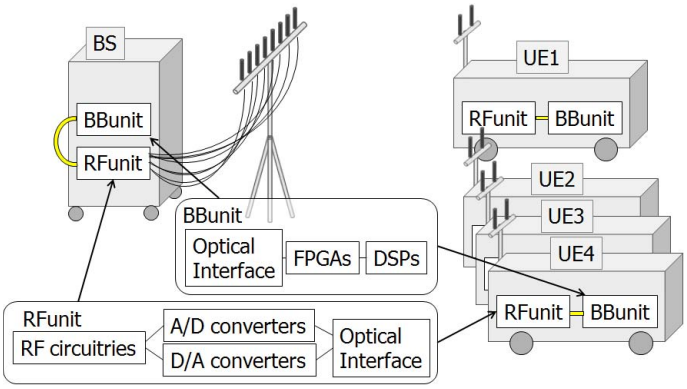

Fig. 1. The overview of the experimental system.

Vector perturbation (VP) [4]–[7], a type of non-linear precoding, has been attracting attention as a promising method of overcoming this problem. To minimize the drop in power efficiency caused by channel correlation, this technique adds an offset vector called a "perturbation vector" to symbols on each stream. This vector can be easily removed at the receiver.

To the best of our knowledge, although there is a report of experiments using a fading simulator about non-linear MU-MIMO adopting Tomlinson-Harashima precoding [8], there have been no report of a field experiment about non-linear MU-MIMO adopting vector perturbation. Accordingly, we constructed an experimental LTE-Advanced-based MU-MIMO system having a maximum configuration of 8×8 antennas to evaluate the performance of vector perturbation [9], [10].

In this paper, we report the results of outdoor and indoor transmission experiments envisioning small-cell environments for which it is thought that a non-linear algorithm would be superior to a linear one, and we compare the throughput obtained by our non-linear algorithm with that of a linear algorithm (MMSE spatial filtering).

II. Experimental System

A. Hardware configuration

Configuration of the experimental system is shown in Fig. 1 and specifications are listed in Table I. This 8×8 MU-MIMO system consists of one BS having an 8-element array antenna and four units of UE having a 2-element array antenna for each. Each UE is mounted on a pushcart with its

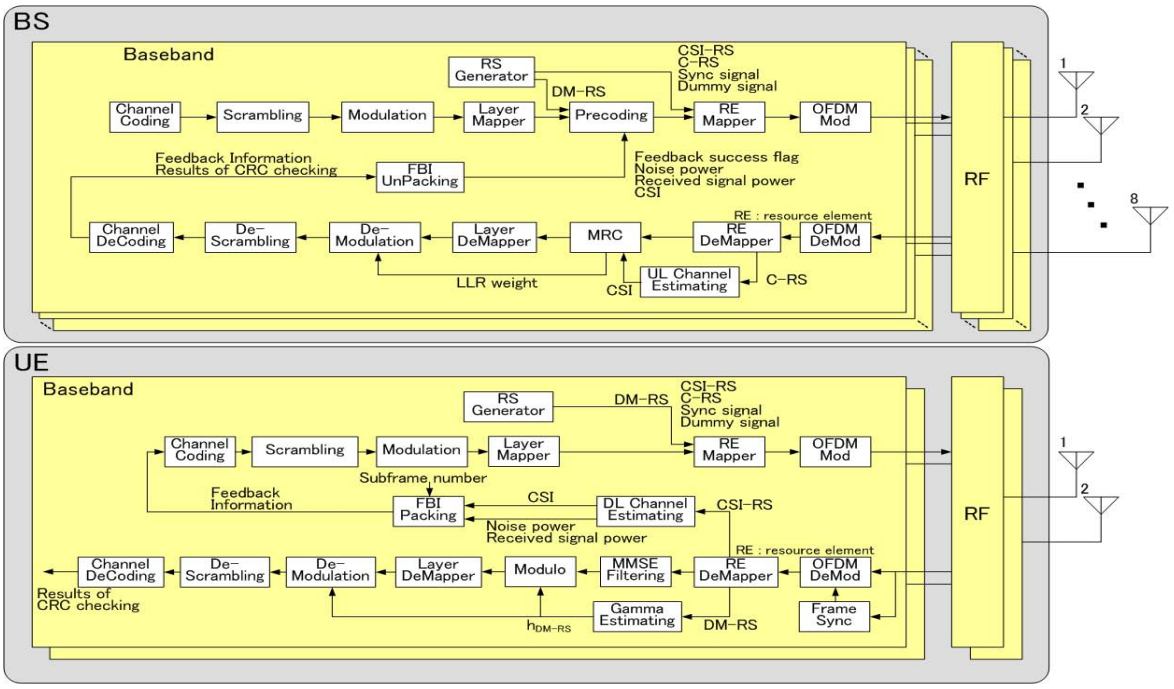

Fig. 2. Baseband block diagram.

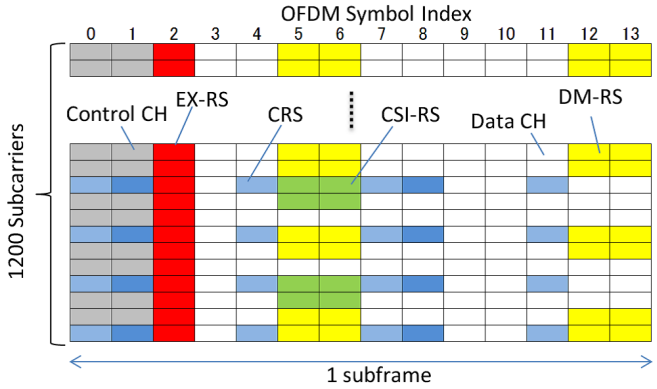

Fig. 3. Subframe format.

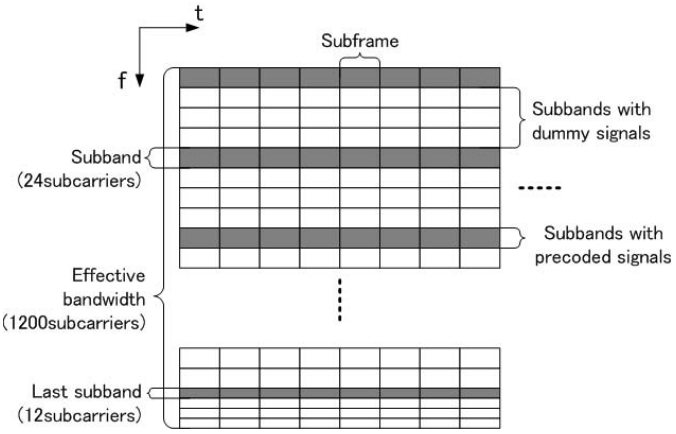

Fig. 4. Subband and resource mapping.

antennas and a power supply unit so that measurements can be performed while an UE is moving. Each antenna element is a monopole antenna having a gain of approximately 2 dBi. Element spacing, polarization-plane angle, and antenna height are variable.

B. Baseband Unit

The block diagram of the baseband unit is shown in Fig. 2. The downlink frame format is based on the 3GPP Release 10 subframe format [11] with some modification as shown in Fig. 3. The demodulation reference signal (DM-RS) is used to demodulate the precoded signal, and the channel state information reference signal (CSI-RS) is used for precoding. It also includes a Zadoff-Chu sequence as an extra reference signal (EX-RS) at the 3rd OFDM symbol for easy timing synchronization and detail channel analysis. They are transmitted every subframe. The system used MU-MIMO-OFDM on the downlink, and OFDMA on the uplink to provide feedback on channel state information. The precoding scheme for transmission used at the BS is MMSE-VP that applies vector perturbation to MMSE spatial filtering as a non-linear algorithm. For comparison purposes, we also implement MMSE spatial filtering without vector perturbation.

As shown in Fig. 4, the 1200 subcarriers are divided into 50 subbands (24 subcarriers per subband) to reduce the CSI feedback load. The last subband has 12 subcarriers. Accordingly the signal has 300 subcarriers over a total of 13 subbands, which is corresponding to a 5-MHz bandwidth signal. In order to realize the real-time processing for the VP technique, we reduce the number of subbands to one-fourth for the purpose of reducing the required computational resources. Here, we apply precoding on every fourth subband so as not to lose the

TABLE I

SPECIFICATIONS

		Base station	User equipment
Base band	Sampling rate	30.72 MHz	
	FFT size	2048	
	Number of subcarriers	1200	
	Length of cyclic prefix	4.7 μsec	
	Number of UEs	4	
	Modulation scheme	QPSK,16QAM,64QAM	
RF	Carrier frequency	3.36 GHz	3.26 GHz
	Transmission power	4 W (MAX)	1 W (MAX)
	Bandwidth	20 MHz	
Antenna	Number of elements	8	2
	Height	1 to 4 m	1 to 3 m

frequency diversity effect.

For searching optimal perturbation vectors, we developed an algorithm based on the QR-decomposition with M-algorithm encode (QRDM-E) technique proposed in the literature [7].

The channel estimation values for the desired signal, which are used in demodulation processing and setting of the modulo-lattice size, are obtained from DM-RS transmitted in each stream by averaging over a subframe.

Channel coefficients used in precoding are obtained by averaging CSI-RS over the last five subframes. Additionally, 8-bit quantization is performed on each I and Q components and fed back to the BS using the data channel on the uplink. Noise variance values required for generating MMSE weights are calculated from CSI-RS and fed back to the BS in the same way. The feedback delay is 7 or 8 ms.

As channel coding, Turbo code shown in the 3GPP Release 10 specification [12] is used. Its decoding scheme is Max Log-MAP with six iterations.

C. Precoding function

We describe the algorithm of K-UE downlink MU-MIMO function utilized in the system. The number of transmission antennas is denoted by N_{t}, and the number of receiving antennas on each UE is denoted by N_{r}. Thus, the number of all receiving antennas becomes KN_{r}.

Notation: $(\cdot)^*$, $(\cdot)^{\mathrm{T}}$ and $(\cdot)^{\mathrm{H}}$ denote complex conjugate, transpose and complex conjugate transpose, respectively. In addition, $j = \sqrt{-1}$. $E[\cdot]$ and $\|\cdot\|^2$ denote ensemble average, and squared Euclidean norm, respectively.

The received signal $\boldsymbol{y} = (y_1, y_2, \ldots, y_{KN_{\mathrm{r}}})^{\mathrm{T}}$ is given by

$$\boldsymbol{y} = \boldsymbol{H}\boldsymbol{z} + \boldsymbol{n}, \tag{1}$$

where $\boldsymbol{z} = (z_1, z_2, \ldots, z_{N_{\mathrm{t}}})^{\mathrm{T}}$ is the precoded transmitted signal, $\boldsymbol{H}$ is a $(KN_{\mathrm{r}} \times N_{\mathrm{t}})$ channel matrix, and $\boldsymbol{n} = (n_1, n_2, \ldots, n_{KN_{\mathrm{r}}})^{\mathrm{T}}$ is a zero mean complex additive white Gaussian noise (AWGN) vector.

1) MMSE spatial filtering: It decouples multiple data streams by multiplying the transmitted symbol $\boldsymbol{x} = (x_1, x_2, \ldots, x_{N_{\mathrm{d}}})^{\mathrm{T}}$ by a precoding matrix $\boldsymbol{W}$ at the transmitter side. Here, we assume that $N_{\mathrm{t}} \leq N_{\mathrm{r}}$. When the number of data streams N_{d} is identical to N_{t}, the precoding matrix $\boldsymbol{W}$ based on MMSE is given as follows

$$\boldsymbol{W} = \tilde{\boldsymbol{H}}^{\mathrm{H}} \left\{ \tilde{\boldsymbol{H}}\tilde{\boldsymbol{H}}^{\mathrm{H}} + \frac{N_{\mathrm{t}}}{\gamma_0}\boldsymbol{I} \right\}^{-1}, \tag{2}$$

where $\tilde{\boldsymbol{H}}$ denotes estimated channel matrix fed back to the transmitter side, $\boldsymbol{I}$ denotes $(KN_{\mathrm{r}} \times KN_{\mathrm{r}})$ unit matrix, and γ_0 is the average received signal-to-noise ratio (SNR). Thus, the transmitted signal $\boldsymbol{z}$ with spatial filtering is given as follows

$$\boldsymbol{z} = \sqrt{\frac{P}{\gamma_{\mathrm{MMSE}}}}\boldsymbol{W}\boldsymbol{x} \tag{3}$$

$$\gamma_{\mathrm{MMSE}} = E\left[\|\boldsymbol{W}\boldsymbol{x}\|^2 \right], \tag{4}$$

where P is the average transmission power. Note that, as Eq. (3) indicates, the received SNR becomes greater as γ_{MMSE} is smaller when the transmission power P is fixed.

2) Vector Perturbation (VP): VP is a precoding scheme which can reduce γ_{MMSE} by employing a technique of dirty-paper coding [4]. As shown in Fig. 5, the VP precoding extends symbol mapping by adding a discrete-valued offset vector, termed a perturbation vector, to modulated symbols. The offset vector $\tilde{\boldsymbol{l}} = (\tilde{l}_1, \tilde{l}_2, \ldots, \tilde{l}_{N_{\mathrm{d}}})^{\mathrm{T}}$ is chosen for each stream according to the modulated symbol vector $\boldsymbol{x}$ so as to minimize a squared Euclidean norm as follows

$$\tilde{\boldsymbol{l}} = \arg\min_{\boldsymbol{l}} E\left[\|\boldsymbol{W}(\boldsymbol{x} + \tau\boldsymbol{l})\|^2 \right] \tag{5}$$

$$l_i = a_i + jb_i \mid (a_i, b_i) \in \{0, \pm 1, \ldots, \pm L\}, \tag{6}$$

where τ is the distance between adjacent two (extended) symbol points which correspond to the same modulated symbol, and L is the integer maximum absolute value of the element in the perturbation vector. Thus, the squared Euclidean norm γ_{VP} is as follows

$$\gamma_{\mathrm{VP}} = E\left[\left\| \boldsymbol{W}\left(\boldsymbol{x} + \tau\tilde{\boldsymbol{l}}\right) \right\|^2 \right]. \tag{7}$$

The transmitted signal with the VP precoding is thus given by

$$\boldsymbol{z} = \sqrt{\frac{P}{\gamma_{\mathrm{VP}}}}\boldsymbol{W}\left(\boldsymbol{x} + \tau\tilde{\boldsymbol{l}}\right). \tag{8}$$

At the receiver side, the constellation of the received signal extended by the perturbation vector are re-mapped onto the

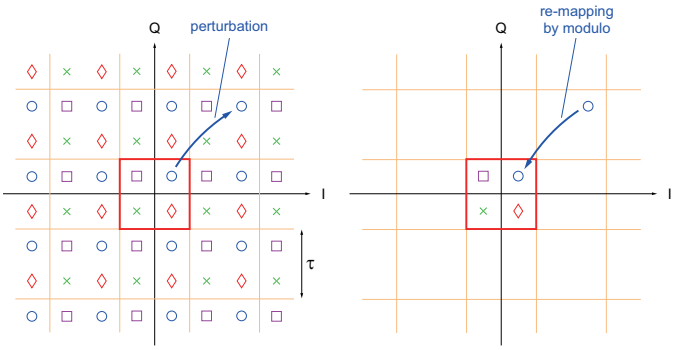

Fig. 5. Example of extended symbol points and re-mapping process. (QPSK modulation)

TABLE II

MODULATION CODING SCHEME PARAMETERS [14]

MCS index	3	4	5	6	7	8
Modulation	QPSK					
Coding rate	0.349	0.44	0.539	0.630	0.747	0.844
TBS	1416	1800	2216	2600	3112	3496
MCS index	10	11	12	13	14	15
Modulation	16QAM					
Coding rate	0.483	0.529	0.597	0.689	0.777	0.869
TBS	4008	4392	4968	5736	6456	7224
MCS index	17	18	19	20	21	22
Modulation	64QAM					
Coding rate	0.620	0.640	0.731	0.792	0.853	0.914
TBS	7736	7992	9144	9912	10680	11448

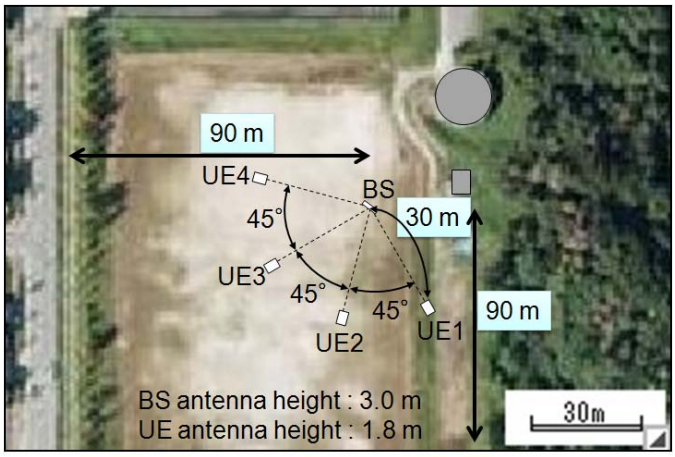

Fig. 6. The arrangement of the BS and UEs for outdoor environment.

regular one as shown in Fig. 5. This process is performed by applying the modulo function to the received signal at each receiving antenna as follows

$$\tilde{y}_i = \left[\left\{ \frac{\hat{g}_i^* y_i}{|\hat{g}_i|} + \frac{\tau'}{2}(1+j) \right\} \mod \tau' \right] - \frac{\tau'}{2}(1+j), \quad (9)$$

where $\hat{g}_i$ denotes channel coefficients after precoding at the i-th receiver antenna element. After this re-mapping process, the received symbol $\tilde{y}_k$ for the k-th data stream are demodulated.

Since $\boldsymbol{HW} \approx \boldsymbol{I}$, the lattice size at the receiver side τ' is assumed as follows [4]

$$\tau' = \sqrt{\frac{P}{\gamma_{\mathrm{VP}}}}\tau. \quad (10)$$

However, in a real system, γ_{VP} is unknown at the receiver side. Therefore we set,

$$\hat{\tau'} = |\hat{g}_i|\,\tau. \quad (11)$$

III. EXPERIMENTAL ENVIRONMENT

To evaluate the performance of vector perturbation, we performed a set of experiments assuming a small-cell environment i.e., outdoor event site. As shown in Fig. 6, we chose a large

Fig. 7. The picture of outdoor environment.

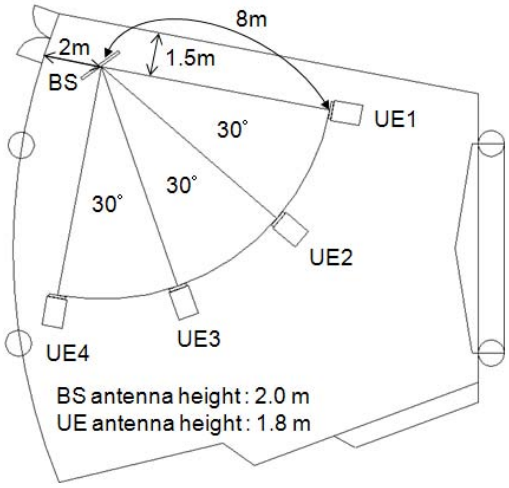

Fig. 8. Indoor experimental setup.

ground of about 90 m × 90 m outdoor area having nearly no reflective objects, and set up four units of UE each at a distance of 30 m from a BS fanned out at intervals of 45 degrees. As shown in Fig. 7, this is a line-of-sight environment with no large reflective objects other than a cylindrical structure and a shed behind the BS. The average received SNRs observed at UE1, UE2, UE3 and UE4 are 21.5 dB, 22.1 dB, 25.3 dB and 25.3 dB, respectively.

Also we performed another set of experiments assuming a small-cell environment such as a large hall which is modeled as an indoor hotspot scenario by WINNER II Channel Models [13]. As shown in Fig. 8, we chose an about 15-m-square lecture hall, and set up four units of UE each at a distance of 8 m from a BS fanned out at intervals of 30 degrees. The average received SNRs observed at UE1, UE2, UE3 and UE4 are 19.1 dB, 18.1 dB, 18.8 dB and 16.5 dB, respectively.

In these environments, we varied the UE antenna configuration (Fig. 10) and measured throughput achieved by

Fig. 9. The picture of indoor environment.

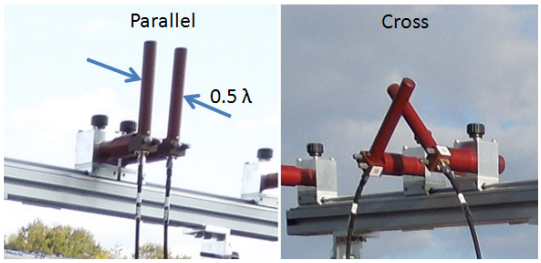

Fig. 10. UE antenna elements configuration.

both MMSE filtering and MMSE-VP for each modulation coding scheme (MCS) index listed in Table II. A crossed UE antenna configuration is expected to improve MIMO channel capacity by decreasing the inter-stream interference depending on antenna correlation and polarization-plane angle.

We observed the channel amplitude of a path from BS antenna element No. 1 (the element closest to UE4) to each UE antenna element using channel coefficients fed back to the BS. Figures 11 and 12 show plots of the ratio of channel amplitude to average amplitude within each subband. Here, the UE antenna element number on the UE1 side is denoted as No. 1 and that on the UE4 side is denoted as No. 2. Frequency fluctuation on the channel of the outdoor environment was within 3 dB. These results show that frequency selectivity of the indoor environment was large compared to the outdoor environment.

IV. Experiment Results

Throughput performances of outdoor environment with parallel antenna, outdoor environment with cross antenna, indoor environment with parallel antenna and indoor environment with cross antenna are shown in Figs. 13, 14, 15 and 16, respectively. Here, "Upper limit" in the figures indicate the upper limit of throughput at a MCS index under error-free condition.

In case of the outdoor environment with the parallel antenna configuration, throughput for both MMSE and MMSE-VP dropped significantly. In the region of MCS index 6 and lower, the difference of throughput between MMSE and MMSE-VP is small. However, in the region of MCS index 7 and higher, throughput of MMSE-VP is relatively larger than that of MMSE.

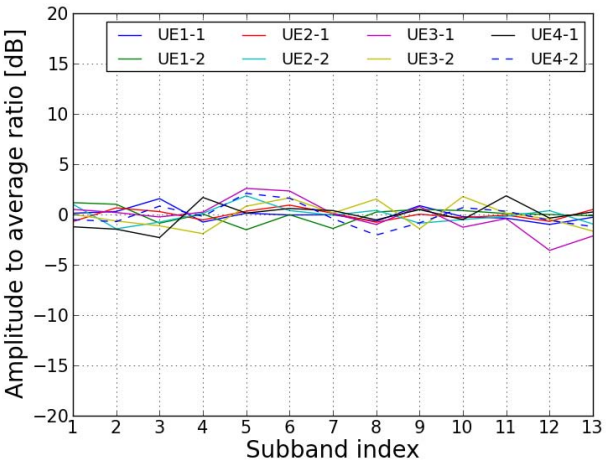

Fig. 11. Channel response of outdoor environment.

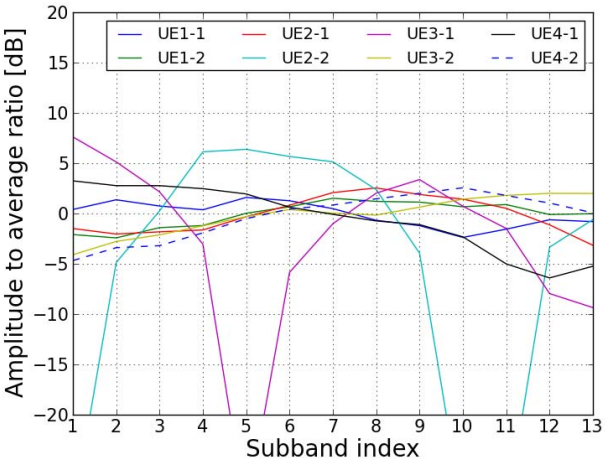

Fig. 12. Channel response of indoor environment.

In case of outdoor environment with the crossed UE antenna configuration, throughput for both MMSE and MMSE-VP are increased. Especially in the region of high-order MCS indexes, throughput for MMSE-VP raised significantly, and maximum throughput of VP (35.3 Mbps at MCS index 12) is 1.72 times higher than that of MMSE (20.5 Mbps at MCS index 6). The reason why MMSE and VP give maximum throughput at different MCS indexes is because the γ_{VP} is smaller than γ_{MMSE} by employing the VP precoding, that is, the received SNR of VP is larger than that of MMSE.

In the indoor environments, MMSE-VP more effectively increased throughput compared to MMSE. MMSE-VP achieved maximum throughputs of 29.6Mbps at MCS index 11 and 40.9Mbps at MCS index 13 while MMSE showed 16.4Mbps at MCS index 5 and 20.7Mbps at MCS index 6 with parallel and cross antenna configurations, respectively. These results mean that maximum throughputs of MMSE-VP achieved 1.81 times and 1.98 times higher than that of MMSE with parallel and cross antenna configurations, respectively.

V. Conclusions

This paper reported results of outdoor and indoor experiments using an 8×8 non-linear MU-MIMO experimental system applying vector perturbation. In the outdoor environment having nearly no reflective objects nearby, throughput for both MMSE and MMSE-VP dropped significantly, but for high-order MCS indexes, vector perturbation obtained a remarkably higher throughput. It was found that in the indoor environment using a crossed UE antenna configuration, there was a large vector-perturbation effect nearly doubling throughput compared to MMSE. In future studies, we plan to perform further analyses to clarify environments where a large vector-perturbation effect can be obtained.

Acknowledgment

This work is supported by the Ministry of Internal Affairs and Communications under a grant entitled "Research and development on nonlinear multiuser MIMO technologies."

References

[1] D. Gesbert, M. Kountouris, R. Heath, C.B. Chae, and T. Salzer, "Shifting the MIMO paradigm," IEEE Signal Processing Mag., vol. 24, no. 5, pp. 36–46, Sept. 2007.

[2] C.B. Peer, B.M. Hochwald, and A.L. Swindlehurst, "A vector-perturbation technique for near-capacity multiantenna multiuser communication — Part I: Channel inversion and regularization," IEEE Trans. Commun., vol. 53, no. 1, pp. 195–202, Jan. 2005.

[3] M.R. McKay, I.B. Collings, and A.M. Tulino, "Achievable sum rate of MIMO MMSE receivers: A general analytic framework," IEEE Trans. Inform. Theory, vol. 56, no. 1, pp. 396–410, Jan. 2010.

[4] B.M. Hochwald, C.B. Peer, and A.L. Swindlehurst, "A vector-perturbation technique for near-capacity multiantenna multiuser communication — Part II: Perturbation," IEEE Trans. Commun., vol. 53, no. 3, pp. 537–544, March 2005.

[5] U. Erez and R. Zamir, "Achieving 1/2log(1+SNR) on the AWGN channel with lattice encoding and decoding," IEEE Trans. Inform. Theory, vol. 50, no. 10, pp. 2293–2314, Oct. 2004.

[6] U. P. Rico, E. Alsusa, and C. Masouros, "A fast least-squares solution-seeker algorithm for vector-perturbation," Proc. of IEEE GLOBECOM 2008, Nov.–Dec. 2008.

[7] M. Mohaisen, B. Hui, K.H. Chang, S. Ji, and J. Joung, "Fixed-complexity vector perturbation with block diagonalization for MU-MIMO systems," Proc. of the 2009 IEEE Malaysia Intl. Conf. on Commun., pp. 238–243, Dec. 2009.

[8] Y. Hatakawa, T. Matsumoto, and S. Konishi, "Development and experiment of linear and non-linear precoding on a real-time multiuser-MIMO testbed with limited CSI feedback," Personal Indoor and Mobile Radio Communications (PIMRC), 2012 IEEE 23rd International Symposium on , vol., no., pp. 1606–1611, Sept. 2012.

[9] S. Tsukamoto, S. Sonobe, T. Maeda, S. Kitazawa, M. Uno, H. Ban, and K. Kobayashi, "An experimental 8×8 MU-MIMO system with block diagonalized vector perturbation," 2012 Thailand-Japan MicroWave (TJMW2012), FR2–2, Aug. 2012.

[10] S. Sonobe, S. Tsukamoto, T. Maeda, K. Yano, H. Ban, M. Uno, and K. Kobayashi, "Outdoor experiments of nonlinear multiuser MIMO transmission with vector perturbation," *IEICE Technical Report*, RCS2012-278, pp. 237–242, Jan. 2013.

[11] 3GPP Technical Specification Group Radio Access Network "Evolved universal terrestrial radio access (E-UTRA); Physical channels and modulation (Release 10)," 3GPP TS36.211 V10.0.0, Dec. 2010.

[12] 3GPP Technical Specification Group Radio Access Network "Evolved universal terrestrial radio access (E-UTRA); Multiplexing and channel coding (Release 10)," 3GPP TS36.212 V10.0.0, Dec. 2010.

[13] "WINNER II channel models, Part I Channel models" IST-4-027756 WINNER II, D1.1.2 V1.2, Feb. 2008.

[14] 3GPP Technical Specification Group Radio Access Network "Evolved universal terrestrial radio access (E-UTRA); Physical layer procedures (Release 10)," 3GPP TS36.213 V10.0.0, Dec. 2010.

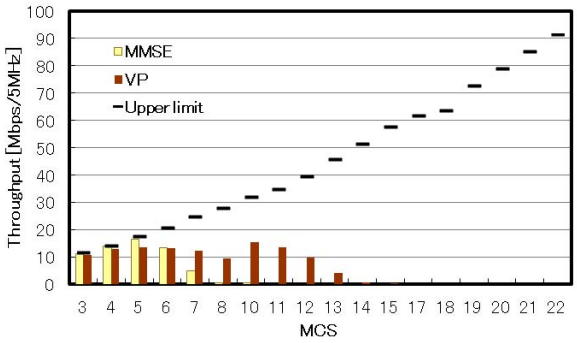

Fig. 13. Throughput in the outdoor environment with the parallel antenna.

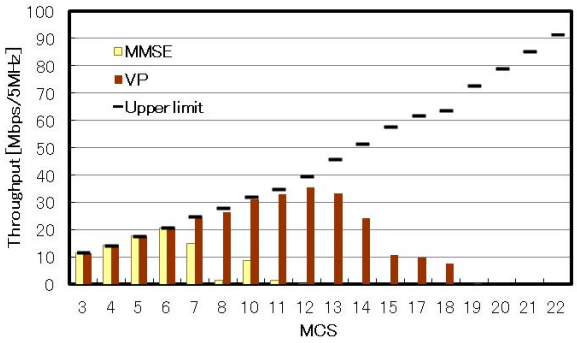

Fig. 14. Throughput in the outdoor environment with the cross antenna.

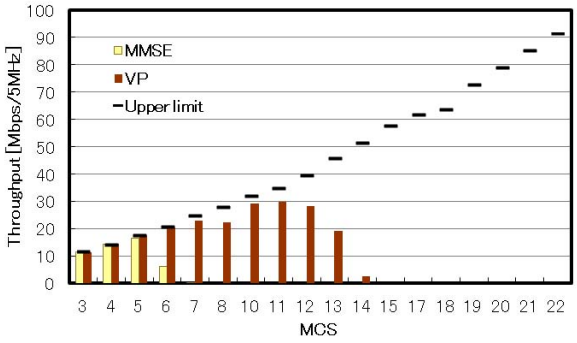

Fig. 15. Throughput in the indoor environment with the parallel antenna.

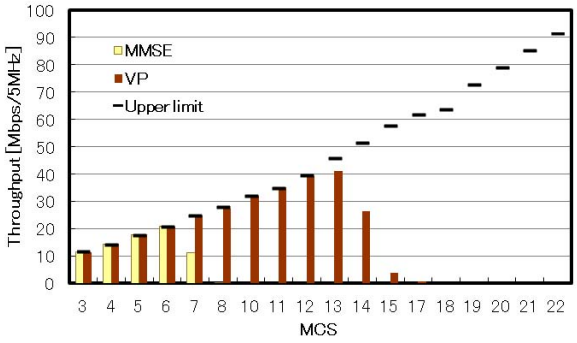

Fig. 16. Throughput in the indoor environment with the cross antenna.